Journal of Magnetic Resonance **136,** 92–101 (1999)
Article ID jmre.1998.1626, available online at http://www.idealibrary.com on IDEAL®

Sensitivity Improvement of Transverse Relaxation-Optimized Spectroscopy

Mark Rance,* J. Patrick Loria,† and Arthur G. Palmer III†

*Department of Molecular Genetics, Biochemistry and Microbiology, University of Cincinnati College of Medicine, 231 Bethesda Avenue, Cincinnati, Ohio 45267-0524; and †Department of Biochemistry and Molecular Biophysics, Columbia University, 630 West 168th Street, New York, New York 10032

Received July 6, 1998; revised September 22, 1998

Procedures are described for significantly improving the sensitivity of the recently proposed TROSY (transverse relaxation-optimized spectroscopy) experiment (K. Pervushin *et al.,* 1997, *Proc. Natl. Acad. Sci. USA* 94, 12366–12371). The TROSY experiment takes advantage of destructive interference between dipolar and chemical shift anisotropy relaxation mechanisms to achieve substantial reductions in resonance linewidths in heteronuclear correlation spectra; the effect is significant particularly for studies of large molecular weight systems at very high static magnetic field strengths. A $\sqrt{2}$ improvement in the sensitivity of the TROSY experiment is achieved by implementation of the PEP (preservation of equivalent pathways) scheme (J. Cavanagh and M. Rance, 1990, *J. Magn. Reson.* 88, 72–85). An additional significant improvement in sensitivity for ^{15}N-labeled samples in H_2O solution is realized through a simple modification of the ^{1}H–^{15}N TROSY pulse sequence to return the water magnetization to its equilibrium position (+z axis) at the beginning of the acquisition period. Relaxation-induced imbalance between the coherence transfer pathways utilized in the TROSY refocusing period is shown theoretically and experimentally to give rise to additional unanticipated signals in TROSY spectra. © 1999 Academic Press

Key Words: **NMR; TROSY; sensitivity improvement; heteronuclear correlation; macromolecules.**

INTRODUCTION

Dramatic increases in spectral resolution and sensitivity in heteronuclear correlation NMR spectroscopy of macromolecules in solution were demonstrated recently by Pervushin and co-workers (*1*). The origin of these improvements lies in the destructive interference between ^{1}H–X dipolar (DD) and the X-nucleus chemical shift anisotropy (CSA) relaxation mechanisms for specific spin-multiplet components (*2*). At very high magnetic field strengths, nearly complete cancellation of the direct dipolar and CSA relaxation processes can be achieved for specific nuclear spin transitions in a heteronuclear AX spin system; consequently, spin–spin relaxation rates for specific multiplet components can be reduced significantly. These interference effects thereby offer the possibility of substantially improved spectral resolution and sensitivity for macromolecules of high molecular mass.

DD–CSA interference, or cross-correlation, in NMR spectroscopy was examined theoretically first by Shimizu (*3*); subsequently, numerous papers have been published that develop more fully the theoretical aspects of DD–CSA cross-correlation and describe practical applications of the measurement of such effects [see (*2*) and references therein]. The influence of DD–CSA interference on resonance linewidths in biomolecular NMR studies was pointed out by Redfield in regard to the nucleic acid work of Guéron *et al.* (*4*). Griffey and Redfield (*5*) anticipated the resolution and sensitivity advantages that could be obtained in heteronuclear correlation spectroscopy through the simple expedient of collecting the data without decoupling in order to realize the benefits of destructive DD–CSA interference. This idea forms the basis of the transverse relaxation-optimized spectroscopy (TROSY) experiment developed by Pervushin *et al.* (*1*).

In the applications for which TROSY-type experiments are most beneficial, sensitivity undoubtedly will be a key issue. Thus, further developments that provide increased sensitivity will have a significant impact on the feasibility of the experiments and the quality of the data recorded. The present paper describes two simple procedures that allow the inherent sensitivity of the original TROSY experiment to be improved by at least 40%, and possibly more; this enhancement reduces the spectrometer time necessary to achieve a particular signal-to-noise figure by at least a factor of 2. The first procedure modifies the manner in which the data are recorded, but does not alter the NMR pulse sequence itself. The second procedure involves a minor modification of the pulse sequence in order to avoid saturation of the solvent resonance. The benefits of these procedures are demonstrated in ^{1}H–^{15}N TROSY experiments on (^{2}H, ^{15}N)-labeled triosephosphate isomerase (TIM), a symmetric dimer with a total molecular mass of 54 kDa (248 amino acid residues per monomer). Details of the TROSY experiment are also illustrated using data recorded for calbindin D_{9k}, a small calcium-binding protein with a molecular mass of 8.5 kDa (75 amino acid residues).

THEORY

A straightforward analysis of the spin dynamics in the TROSY experiment described by Pervushin *et al.* (*1*) indicates that a $\sqrt{2}$

1090-7807/99 $30.00
Copyright © 1999 by Academic Press
All rights of reproduction in any form reserved.

improvement in sensitivity immediately can be achieved via the implementation of the PEP (preservation of equivalent pathways) method that has been widely applied in numerous experiments such as homonuclear TOCSY (*6, 7*) and various heteronuclear correlation experiments (*8–13*). PEP is a general approach whereby a conventional pulse sequence for a desired experiment is redesigned to preserve two essentially equivalent coherence transfer pathways. The signals from the two pathways are recorded simultaneously and separated after acquisition as part of the data processing protocol. In one approach, the two signals are processed to obtain two identical spectra with the same sensitivity as a conventional experiment recorded in the same total time and the improved sensitivity is obtained by adding the two independent spectra (*6, 7*). In an alternative approach, the two signals are used as a complex pair to provide frequency discrimination in the relevant indirect dimension of the multidimensional experiment (*11, 12*). This procedure obviates the need for separate collection of a phase-shifted orthogonal data set for frequency discrimination and results in identical sensitivity in half the acquisition time required for a conventional experiment. In either case, a sensitivity improvement by a factor up to $\sqrt{2}$ per unit time is achieved for each frequency dimension in which the PEP procedure can be applied. The practical implementation of the PEP methodology depends on the details of individual experiments. In some cases, no change in the actual pulse sequence is necessary (*6*), whereas other cases require some reengineering of the original pulse sequence (*7–12*). If the original pulse sequence must be lengthened to implement the PEP method, then additional relaxation effects can reduce the actual sensitivity gain below $\sqrt{2}$ (*7, 8*).

The TROSY experiment of Pervushin and co-workers already is suited ideally for implementation of the PEP procedure, and no changes in the actual pulse sequence are necessary. PEP is implemented in TROSY simply by separating the phase-cycling steps into two halves, and accumulating the data separately for the two reduced phase cycles. For the convenience of the present discussion, the original TROSY pulse sequence, with the phase of the first proton 180° pulse changed from x to y (*vide infra*), is reproduced in Fig. 1a. In order to demonstrate how the PEP enhancement is achieved, a detailed analysis of the spin dynamics during the pulse sequence is useful.

The theoretical treatment of coherence transfer and relaxation effects during the TROSY experiment parallels the analysis performed for PEP sensitivity enhancement of other heteronuclear correlation experiments (*7, 8*). The Cartesian basis product operators with $I = {}^1\mathrm{H}$ and $S = {}^{15}\mathrm{N}$ are utilized to represent the evolution of the density operator through the pulse sequence (*14–17*). For clarity, the relaxation decay functions for the individual multiplet components during the evolution period t_1 are not shown; these are given in (*1*) and do not affect the present analysis. Only components of the density operator originating with proton spin polarization are considered. The small contribution to the density operator and detected signal from ${}^{15}\mathrm{N}$ spin polarization is ignored for simplicity; however, the effects of relaxation on these components of the density operator can be analyzed analogously. Unlike most heteronuclear correlation experiments, signals arising from the original ${}^{15}\mathrm{N}$ spin polarization contribute constructively to the desired TROSY spectra and should be preserved in the experiment (*1*).

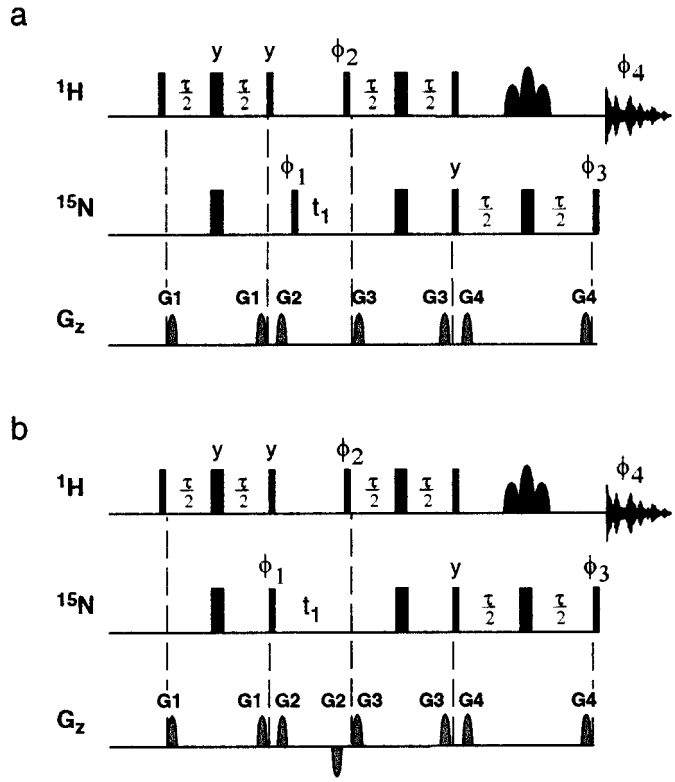

FIG. 1. Pulse sequences for (a) the original TROSY experiment (*1*) and (b) a TROSY experiment modified to incorporate water flip-back. Narrow and thick bars represent RF pulses with 90° and 180° nominal flip angles, respectively; all pulses have phase $+x$ unless otherwise indicated. The final proton composite 180° pulse is part of a WATERGATE (*27*) scheme, and thus is designed to nominally be a 180° pulse for the spectral region of interest and a 0° or 360° pulse for the water magnetization. Either the originally proposed 90°_x(selective)–180°_{-x}(nonselective)–90°_x(selective) composite sequence (*27*) or crafted composite 180° pulses such as the so-called 3–9–19 sequence (*25*) can be used. For sequence (b) the proton transmitter frequency must be placed at the water resonance frequency to achieve the desired flip-back of the water magnetization at the end of the t_1 period. Bipolar gradients G2 are inserted in the t_1 period of sequence (b) to minimize radiation damping. The delay $\tau = 0.5/J_{\mathrm{NH}}$. To implement the PEP scheme for sensitivity enhancement, the conventional phase cycle is divided into two halves, with separate recording of the two FIDs. For experiments performed on Varian INOVA spectrometers (see text for changes required for a Bruker DRX spectrometer), the first FID is recorded with $\phi_1 = (+y, -y, -x, +x)$, $\phi_2 = +y$, $\phi_3 = +x$, and $\phi_4 = (+x, -x, +y, -y)$, while the second FID is acquired with $\phi_1 = (+y, -y, -x, +x)$, $\phi_2 = -y$, $\phi_3 = -x$, and $\phi_4 = (-x, +x, +y, -y)$. The required data processing for the PEP scheme is described in the text. The magnetic field gradient pulses are: (a) G1, amplitude = 5 G/cm, duration = 400 μs; G2 = 20 G/cm, 1 ms; G3 = 5 G/cm, 400 μs; G4 = 12 G/cm, 400 μs; and (b) G1 = 5 G/cm, 400 μs, G2 = 4 G/cm, 320 μs; G3 = 5 G/cm, 400 μs; G4 = 12 G/cm, 400 μs. The G2 gradient pulse in sequence (b) should be set at a level sufficient to prevent significant radiation damping of the water magnetization during the t_1 period.

Prior to the first ${}^{15}\mathrm{N}$ 90° pulse of phase ϕ_1 (see Fig. 1a), the density operator is given by

$$\sigma(0) = -2I_zS_z. \qquad [1]$$

For the first step of the phase cycle given in the legend to Fig. 1, $\phi_1 = y$ and the density operator after the t_1 period is given by

$$\begin{aligned}\sigma(t_1) = &-2I_zS_x\cos(\pi J_{\mathrm{NH}}t_1)\cos(\Omega_{\mathrm{N}}t_1)\\ &- S_y\sin(\pi J_{\mathrm{NH}}t_1)\cos(\Omega_{\mathrm{N}}t_1)\\ &- 2I_zS_y\cos(\pi J_{\mathrm{NH}}t_1)\sin(\Omega_{\mathrm{N}}t_1)\\ &+ S_x\sin(\pi J_{\mathrm{NH}}t_1)\sin(\Omega_{\mathrm{N}}t_1)\end{aligned} \quad [2]$$

in which J_{NH} is the one-bond N–H scalar coupling constant and Ω_{N} is the chemical shift of the ^{15}N spin.

Direct analysis of the TROSY refocusing period (beginning with the 90° ^{1}H pulse following the t_1 period and ending with the final ^{15}N 90° pulse prior to acquisition) yields the following effective propagator,

$$\begin{aligned}\mathbf{U} = &\exp\left(-i\,\frac{\pi}{2}\,S_{\phi3}\right)\exp\left(-i\,\frac{\pi}{2}\,2I_zS_z\right)\exp\left(-i\,\frac{\pi}{2}\,I_x\right)\\ &\times\exp\left(i\,\frac{\pi}{2}\,S_y\right)\exp\left(-i\,\frac{\pi}{2}\,2I_zS_z\right)\exp\left(-i\,\frac{\pi}{2}\,I_{\phi2}\right)\end{aligned} \quad [3]$$

in which $\tau = 1/(2J_{\mathrm{NH}})$ has been assumed. For the first step of the phase cycle, the density operator given by Eq. 2 evolves through the TROSY refocusing period as

$$\begin{aligned}\sigma(t_1) \xrightarrow{\pi/2\ I_y}\ &-2I_xS_x\cos(\pi J_{\mathrm{NH}}t_1)\cos(\Omega_{\mathrm{N}}t_1)\\ &- S_y\sin(\pi J_{\mathrm{NH}}t_1)\cos(\Omega_{\mathrm{N}}t_1)\\ &- 2I_xS_y\cos(\pi J_{\mathrm{NH}}t_1)\sin(\Omega_{\mathrm{N}}t_1)\\ &+ S_x\sin(\pi J_{\mathrm{NH}}t_1)\sin(\Omega_{\mathrm{N}}t_1)\\ \xrightarrow{\pi/2\ 2I_zS_z}\ &-2I_xS_x\cos(\pi J_{\mathrm{NH}}t_1)\cos(\Omega_{\mathrm{N}}t_1)\exp(-R_{\mathrm{MQ}}\tau)\\ &+ 2I_zS_x\sin(\pi J_{\mathrm{NH}}t_1)\cos(\Omega_{\mathrm{N}}t_1)\exp(-R_{2\mathrm{S}}\tau)\\ &- 2I_xS_y\cos(\pi J_{\mathrm{NH}}t_1)\sin(\Omega_{\mathrm{N}}t_1)\exp(-R_{\mathrm{MQ}}\tau)\\ &+ 2I_zS_y\sin(\pi J_{\mathrm{NH}}t_1)\sin(\Omega_{\mathrm{N}}t_1)\exp(-R_{2\mathrm{S}}\tau)\\ \xrightarrow{\pi/2\ I_x,\ -\pi/2\ S_y}\ &-2I_xS_z\cos(\pi J_{\mathrm{NH}}t_1)\cos(\Omega_{\mathrm{N}}t_1)\exp(-R_{\mathrm{MQ}}\tau)\\ &- 2I_yS_z\sin(\pi J_{\mathrm{NH}}t_1)\cos(\Omega_{\mathrm{N}}t_1)\exp(-R_{2\mathrm{S}}\tau)\\ &- 2I_xS_y\cos(\pi J_{\mathrm{NH}}t_1)\sin(\Omega_{\mathrm{N}}t_1)\exp(-R_{\mathrm{MQ}}\tau)\\ &- 2I_yS_y\sin(\pi J_{\mathrm{NH}}t_1)\sin(\Omega_{\mathrm{N}}t_1)\exp(-R_{2\mathrm{S}}\tau)\\ \xrightarrow{\pi/2\ 2I_zS_z}\ &-I_y\cos(\pi J_{\mathrm{NH}}t_1)\cos(\Omega_{\mathrm{N}}t_1)\exp(-[R_{\mathrm{MQ}} + R_{2\mathrm{I}}]\tau)\\ &+ I_x\sin(\pi J_{\mathrm{NH}}t_1)\cos(\Omega_{\mathrm{N}}t_1)\exp(-[R_{2\mathrm{S}} + R_{2\mathrm{I}}]\tau)\\ &- 2I_xS_y\cos(\pi J_{\mathrm{NH}}t_1)\sin(\Omega_{\mathrm{N}}t_1)\exp(-2R_{\mathrm{MQ}}\tau)\\ &- 2I_yS_y\sin(\pi J_{\mathrm{NH}}t_1)\sin(\Omega_{\mathrm{N}}t_1)\exp(-[R_{2\mathrm{S}} + R_{\mathrm{MQ}}]\tau)\\ \xrightarrow{\pi/2\ S_x}\ &-I_y\cos(\pi J_{\mathrm{NH}}t_1)\cos(\Omega_{\mathrm{N}}t_1)\exp(-[R_{\mathrm{MQ}} + R_{2\mathrm{I}}]\tau)\\ &+ I_x\sin(\pi J_{\mathrm{NH}}t_1)\cos(\Omega_{\mathrm{N}}t_1)\exp(-[R_{2\mathrm{S}} + R_{2\mathrm{I}}]\tau)\\ &- 2I_xS_z\cos(\pi J_{\mathrm{NH}}t_1)\sin(\Omega_{\mathrm{N}}t_1)\exp(-2R_{\mathrm{MQ}}\tau)\\ &- 2I_yS_z\sin(\pi J_{\mathrm{NH}}t_1)\sin(\Omega_{\mathrm{N}}t_1)\exp(-[R_{2\mathrm{S}} + R_{\mathrm{MQ}}]\tau)\end{aligned} \quad [4]$$

in which exponential damping of the amplitudes of single-quantum ^{1}H coherences, single-quantum ^{15}N coherences, and multiple-quantum coherences during the delays τ have been included in the expressions for the density operator.

The relaxation rate constants for single-quantum ^{1}H coherence, single-quantum ^{15}N coherence, and multiple-quantum coherence are given by (*17, 18*)

$$\begin{aligned}R_{2\mathrm{I}} = &(d_{IS}^2/8)[4J(0) + J(\omega_I - \omega_S) + 3J(\omega_I)\\ &+ 3J(\omega_S) + 6J(\omega_I + \omega_S)]\\ &+ (c_I^2/6)[4J(0) + 3J(\omega_I)] + (c_S^2/2)J(\omega_S)\\ &+ \sum_K (d_{IK}^2/8)[5J(0) + 9J(\omega_I) + 6J(2\omega_I)]\end{aligned} \quad [5]$$

$$\begin{aligned}R_{2\mathrm{S}} = &(d_{IS}^2/8)[4J(0) + J(\omega_I - \omega_S) + 3J(\omega_S)\\ &+ 3J(\omega_I) + 6J(\omega_I + \omega_S)]\\ &+ (c_S^2/6)[4J(0) + 3J(\omega_S)] + (c_I^2/2)J(\omega_I)\\ &+ \sum_K (d_{IK}^2/8)[J(0) + 3J(\omega_I) + 6J(2\omega_I)]\end{aligned} \quad [6]$$

$$\begin{aligned}R_{\mathrm{MQ}} = &(d_{IS}^2/8)[J(\omega_I - \omega_S) + 3J(\omega_S)\\ &+ 3J(\omega_I) + 6J(\omega_I + \omega_S)]\\ &+ (c_I^2/6)[4J(0) + 3J(\omega_I)]\\ &+ (c_S^2/6)[4J(0) + 3J(\omega_S)]\\ &+ \sum_K (d_{IK}^2/8)[5J(0) + 9J(\omega_I) + 6J(2\omega_I)]\end{aligned} \quad [7]$$

in which

$$d_{IJ} = \gamma_I\gamma_J h\mu_0 r_{IJ}^{-3}/(8\pi^2) \quad [8]$$

$$c_J = \omega_J\Delta\sigma_J/\sqrt{3}. \quad [9]$$

μ_0 is the permittivity of free space; h is Planck's constant; γ_I and γ_S are the gyromagnetic ratios of the I and S spins, respectively; r_{IS} is the length of the IS bond; r_{IK} is the distance between the amide proton and a remote proton K; ω_I and ω_S are the Larmor frequencies of the ^{1}H and ^{15}N spins, respectively; and $\Delta\sigma_I$ and $\Delta\sigma_S$ are the chemical shift anisotropies of the (assumed axial) ^{1}H

and ^{15}N chemical shift tensors, respectively. For a rigid, isotropic rotor, the spectral density function is given by $J(\omega) = (2/5)\tau_m/(1 + \omega^2\tau_m^2)$, in which τ_m is the rotational correlation time of the molecule. The expressions given for R_{2I} and R_{2S} include the effect of averaging between in-phase and antiphase operators during the period τ (*19*) and the expressions for all three rate constants contain contributions from remote protons. The summations include all remote protons ($K \neq I$) in the protein and will depend on whether the nonexchangeable protons have been replaced with deuterons. The effects of methyl group rotations and aromatic ring flips on the amide ^{1}H relaxation have not been included for simplicity (*17*).

By the same approach, the summed density operator present immediately prior to acquisition (but including receiver phase shifts) for the first four steps of the phase cycle is

$$\begin{aligned}\sigma_P = &-2I_y[\cos(\pi J_{NH}t_1)\cos(\Omega_N t_1)\exp(-[R_{MQ} + R_{2I}]\tau)\\ &- \sin(\pi J_{NH}t_1)\sin(\Omega_N t_1)\exp(-[R_{2S} + R_{2I}]\tau)]\\ &+ 2I_x[\cos(\pi J_{NH}t_1)\sin(\Omega_N t_1)\exp(-[R_{MQ} + R_{2I}]\tau)\\ &+ \sin(\pi J_{NH}t_1)\cos(\Omega_N t_1)\exp(-[R_{2S} + R_{2I}]\tau)]\\ &+ 4I_y S_z[\cos(\pi J_{NH}t_1)\cos(\Omega_N t_1)\exp(-2R_{MQ}\tau)\\ &- \sin(\pi J_{NH}t_1)\sin(\Omega_N t_1)\exp(-[R_{2S} + R_{MQ}]\tau)]\\ &- 4I_x S_z[\cos(\pi J_{NH}t_1)\sin(\Omega_N t_1)\exp(-2R_{MQ}\tau)\\ &+ \sin(\pi J_{NH}t_1)\cos(\Omega_N t_1)\exp(-[R_{2S} + R_{MQ}]\tau)].\end{aligned} \quad [10]$$

The density operator obtained for the last four steps of the phase cycle is

$$\begin{aligned}\sigma_N = &-2I_y[\cos(\pi J_{NH}t_1)\cos(\Omega_N t_1)\exp(-[R_{MQ} + R_{2I}]\tau)\\ &- \sin(\pi J_{NH}t_1)\sin(\Omega_N t_1)\exp(-[R_{2S} + R_{2I}]\tau)]\\ &- 2I_x[\cos(\pi J_{NH}t_1)\sin(\Omega_N t_1)\exp(-[R_{MQ} + R_{2I}]\tau)\\ &+ \sin(\pi J_{NH}t_1)\cos(\Omega_N t_1)\exp(-[R_{2S} + R_{2I}]\tau)]\\ &+ 4I_y S_z[\cos(\pi J_{NH}t_1)\cos(\Omega_N t_1)\exp(-2R_{MQ}\tau)\\ &- \sin(\pi J_{NH}t_1)\sin(\Omega_N t_1)\exp(-[R_{2S} + R_{MQ}]\tau)]\\ &+ 4I_x S_z[\cos(\pi J_{NH}t_1)\sin(\Omega_N t_1)\exp(-2R_{MQ}\tau)\\ &+ \sin(\pi J_{NH}t_1)\cos(\Omega_N t_1)\exp(-[R_{2S} + R_{MQ}]\tau)]\end{aligned} \quad [11]$$

in which σ_P and σ_N represent density operators resulting in echo and antiecho signals, respectively.

The P- and N-type signals represented by Eqs. [10] and [11] are acquired and stored separately in the PEP scheme. The real component of the F1 quadrature signal, represented by σ_R, is obtained by summing the signals represented by Eqs. [10] and [11] after acquisition:

$$\begin{aligned}\sigma_R = &-4I_y[\cos(\pi J_{NH}t_1)\cos(\Omega_N t_1)\exp(-[R_{MQ} + R_{2I}]\tau)\\ &- \sin(\pi J_{NH}t_1)\sin(\Omega_N t_1)\exp(-[R_{2S} + R_{2I}]\tau)]\\ &+ 8I_y S_z[\cos(\pi J_{NH}t_1)\cos(\Omega_N t_1)\exp(-2R_{MQ}\tau)\\ &- \sin(\pi J_{NH}t_1)\sin(\Omega_N t_1)\exp(-[R_{2S} + R_{MQ}]\tau)].\end{aligned} \quad [12]$$

The imaginary component, represented by σ_I, is obtained by subtracting the signals represented by Eqs. [10] and [11] after acquisition:

$$\begin{aligned}\sigma_I = &\ 4I_x[\cos(\pi J_{NH}t_1)\sin(\Omega_N t_1)\exp(-[R_{MQ} + R_{2I}]\tau)\\ &+ \sin(\pi J_{NH}t_1)\cos(\Omega_N t_1)\exp(-[R_{2S} + R_{2I}]\tau)]\\ &- 8I_x S_z[\cos(\pi J_{NH}t_1)\sin(\Omega_N t_1)\exp(-2R_{MQ}\tau)\\ &+ \sin(\pi J_{NH}t_1)\cos(\Omega_N t_1)\exp(-[R_{2S} + R_{MQ}]\tau)].\end{aligned} \quad [13]$$

The above analysis demonstrates that, aside from minor effects due to possible pulse imperfections, the basic TROSY pulse sequence provides two equivalent coherence transfer pathways leading to the NMR signals of interest. The phase difference between the two signal components in the acquisition dimension (represented by the I_y and I_x operators in Eqs. [12] and [13]) is corrected trivially by applying a 90° phase correction in F2 or by performing equivalent manipulations in the time domain for one of the two data sets (*7*). The data set represented by σ_R is cosine-modulated and the data set represented by σ_I is sine-modulated with respect to the ^{15}N chemical shift during t_1. Therefore, the two data sets can be processed by the conventional hypercomplex approach (*17, 20*) to obtain absorption mode lineshapes in both frequency dimensions. The signal-to-noise ratio is identical to that obtained by recording conventional hypercomplex data using the original eight-step phase cycle and shifting the phase of ϕ_1 by 90° to obtain each member of the quadrature pair in F1 (*1*). Consequently, the total acquisition time for the sensitivity-enhanced experiment, relative to the conventional experiment, is reduced by half without affecting sensitivity.

As can be seen in the analysis above, the effects of relaxation are identical for the real and imaginary components of the F1 quadrature pair; thus, only the real part needs to be considered further to illustrate the effects of relaxation during the TROSY refocusing period on the final spectrum. The exponential terms in Eq. [12] can be expanded to first order in τ, under the assumption that the rates are much less than $1/(4\tau)$ ($\ll 100$ s^{-1}). The final expression obtained from Eq. [12] is

$$\sigma_R = -4(I_y - 2I_yS_z)\cos[(\Omega_N + \pi J_{NH})t_1]\epsilon_1 - 4(I_y - 2I_yS_z)\cos[(\Omega_N - \pi J_{NH})t_1]\epsilon_2 - 4(I_y + 2I_yS_z)\cos[(\Omega_N + \pi J_{NH})t_1]\epsilon_3 \quad [14]$$

in which

$$\epsilon_1 = 1 - (2R_{MQ} + R_{2I} + R_{2S})\tau/2 \quad [15]$$

$$\epsilon_2 = (R_{2S} - R_{MQ})\tau/2 \approx 2J(0)\tau[d_{IS}^2/8 - c_I^2/6 - \sum_K d_{IK}^2/8] \quad [16]$$

$$\epsilon_3 = (R_{MQ} - R_{2I})\tau/2 = 2J(0)\tau[-d_{IS}^2/8 + c_S^2/6] \quad [17]$$

are the amplitude of the TROSY peak at frequency coordinates ($\Omega_N + \pi J_{NH}$, $\Omega_H - \pi J_{NH}$) as reduced by relaxation losses during the refocusing period, the amplitude of the multiplet component at frequency coordinates ($\Omega_N - \pi J_{NH}$, $\Omega_H - \pi J_{NH}$), and the amplitude of the multiplet component at ($\Omega_N + \pi J_{NH}$, $\Omega_H + \pi J_{NH}$), respectively. The fourth multiplet component at ($\Omega_N - \pi J_{NH}$, $\Omega_H + \pi J_{NH}$) is identically zero to first order. The rightmost expression in Eq. [16] is obtained assuming that $J(0) \gg J(\omega_I)$ for macromolecules. If the relaxation rate constants R_{2I}, R_{2S}, and R_{MQ} are identical, then only the desired TROSY resonance appears in the spectrum. An additional resonance with amplitude ϵ_2 results from the relaxation-induced imbalance between the two terms contributing to the amplitude of the I_y operator or between the two terms contributing to the $2I_yS_z$ operator in Eq. [12]; an additional resonance with amplitude ϵ_3 results from the relaxation-induced imbalance between the I_y and $2I_yS_z$ operators in Eq. [12]. At high field, for which TROSY experiments are optimal, $d_{IS}^2/8 \approx c_S^2/6 \approx c_I^2/6$ and $R_{MQ} \approx R_{2I}$. Consequently, the resonance represented by ϵ_3 is expected to be small in all circumstances with an amplitude that depends on the static magnetic field strength. In contrast, $R_{2S} - R_{MQ}$ is dominated by the larger contribution to R_{MQ} from dipolar interactions with the remote protons. Therefore, the amplitude of the multiplet component represented by ϵ_2 will depend upon whether the nonexchangeable protons in the molecule have been replaced by deuterons. The intensity decay of the desired TROSY signal due to relaxation reflected by ϵ_1 also is dominated by the contributions to relaxation from dipolar interactions between the amide proton and remote protons and can be reduced by deuteration.

In addition to the $\sqrt{2}$ sensitivity enhancement provided by the implementation of the PEP methodology, further improvements can be achieved in ^{1}H–^{15}N TROSY experiments for aqueous samples by modifying the pulse sequence to avoid water saturation. Since Grzesiek and Bax (*21*) and Stonehouse *et al.* (*22*) initially discussed the advantage of "water flip-back" methods that return the water proton magnetization to the $+z$ axis (as defined by the external B_0 field) at the beginning of the acquisition period, other groups have reported modifications of various pulse sequences designed to achieve the same result (*23, 24*). One of the most effective procedures for water flip-back in HSQC experiments was proposed by Mori *et al.* (*24*). The so-called FHSQC pulse sequence minimizes radiation damping effects, which can degrade the quality of water suppression, and does not require selective 90° water flip-back pulses, which can introduce unnecessary delays into the pulse sequence. In the FHSQC sequence, a gradient pulse is applied during the first INEPT segment when the desired coherences are stored as $2I_zS_z$ spin order. This gradient defocuses the transverse H_2O magnetization. Subsequently, a second gradient pulse in the corresponding period of the reverse INEPT segment refocuses the H_2O magnetization, and the following ^{1}H 90° pulse returns the magnetization to the $+z$ axis. A crafted ^{1}H 180° pulse, such as the common 3–9–19 composite pulse (*25*) or variations thereof (*26*), replaces the final nonselective pulse normally used in the reverse INEPT. The crafted pulse is tuned to provide the necessary excitation bandwidth for the amide proton resonances and a null at the H_2O frequency. In practice this method provides superior suppression of the water signal, compared to the alternative of placing the water magnetization along the $-z$ axis with the final ^{1}H 90° pulse and rotating it back up to the $+z$ axis with a nonselective ^{1}H 180° pulse, because deleterious effects of radiation damping during the reverse INEPT are avoided.

Modification of the TROSY experiment to eliminate water saturation and leave the water magnetization along the $+z$ axis at the beginning of the detection period is easily achieved, as shown in Fig. 1b, using the same general idea as proposed by Mori *et al.* (*24*). A magnetic field gradient pulse just after the first 90° ^{15}N pulse causes the solvent magnetization to be dephased during the t_1 period; at the end of the t_1 period, a second gradient pulse of opposite amplitude is used to refocus the solvent magnetization. A straightforward vector analysis of the subsequent sequence of proton pulses demonstrates that the water magnetization is returned to the $+z$ axis by the final ^{1}H 90° pulse, and is unperturbed by the following application of a 3–9–19 (or similar) ^{1}H composite 180° pulse. The original WATERGATE-type sequence (*27*) could also be used in place of the 3–9–19 pulse. No gradient is applied when the coherences of interest are stored as $2I_zS_z$ spin order; consequently, relaxation losses associated with this gradient and eddy current recovery delay in the original pulse sequence of Fig. 1a are avoided. If the initial t_1 value is set to half of the dwell time (*28*), sufficient time may not be available to accommodate the defocusing and refocusing gradient pulses and associated eddy current recovery delays within the initial t_1 delay, particularly for the larger spectral widths necessary at very high magnetic field strengths. The pair of gradient pulses in the t_1 period do not affect the desired ^{15}N single-quantum coherences present at the end of the t_1 period; consequently, the gradient pair simply can be omitted from the sequence until t_1 has been incremented to a value large enough to encompass the gradients.

EXPERIMENTAL

Experimental data to demonstrate the sensitivity improvements described above were recorded using samples of ^{15}N-labeled calbindin D_{9k} (4 mM, pH 5.5) in 90% H_2O/10% D_2O solution and (^{2}H, ^{15}N)-labeled TIM in 90% H_2O/10% D_2O buffer solution (2 mM TIM, 10 mM CD_3CO_2Na, 0.02% NaN_3, pH 5.7). The ^{15}N-labeled calbindin sample was a gift from Dr. Walter Chazin (Scripps Research Institute). The (W90Y, W157F) double mutant of yeast TIM was overexpressed using the *Escherichia coli* strain JM105 (Pharmacia) transformed with a *tac* promoter expression plasmid (pK223-C, Pharmacia) containing the coding sequence for the protein. The plasmid was a gift from Dr. Ann McDermott of Columbia University. The JM105 cells were acclimated to growth in 67% deuterated media and then the protein was overexpressed using M9 minimal medium (*29*) containing 1.85 g/L $^{15}NH_4Cl$, 1% glucose (natural ^{1}H and ^{12}C abundance), 1 g/L thiamine, 0.45 g/L biotin, 0.05 mM $CaCl_2$, 0.5 mM $MgSO_4$, 0.05 mM $CuCl_2$, 125 μg/ml ampicillin, and 5 mM IPTG prepared in 99% D_2O. TIM was purified essentially as described (*30*) except that cells were lysed by sonication and the final chromatography step was performed using a High-Q ion exchange column (Bio-Rad). Purified TIM migrated as a single band on SDS–PAGE with a MW of 27 kDa and was judged to be >95% pure. Enzymatic activity of purified TIM was quantitated according to the method described by Knowles and co-workers (*31*). Kinetic constants, V_{max} and k_{cat}, were identical to values previously published for wild-type and (W90Y, W157F) mutant TIM (not shown) (*30, 32*). The extent of deuterium incorporation was determined by MALDI-TOF mass spectrometry (University of Michigan Protein and Carbohydrate Structure Facility) to be 45%.

The NMR experiments were performed on INOVA 500- and 800-MHz spectrometers, and the data processing was performed using the Felix software package (Molecular Simulations, Inc.) and in-house written programs. To implement the PEP procedure, data are recorded separately for the two halves of the original eight-step phase cycle; i.e., for each value of t_1, a FID is recorded with $\phi_1 = (+y, -y, -x, +x)$, $\phi_2 = +y$, $\phi_3 = +x$, and $\phi_4 = (+x, -x, +y, -y)$, and then a second FID is recorded with $\phi_1 = (+y, -y, -x, +x)$, $\phi_2 = -y$, $\phi_3 = -x$, and $\phi_4 = (-x, +x, +y, -y)$. Processing of the PEP sensitivity-enhanced TROSY data is simplified if the hypercomplex method (*17, 20*) is employed for F1 quadrature detection in a manner identical to that used in the gradient-enhanced HSQC experiment proposed by Kay *et al.* (*11*). Two new FIDs are created by taking the sum and difference of the original data. As shown by Eqs. [12] and [13], these new FIDs have pure sine or cosine modulation with respect to t_1. The real and imaginary parts of one FID are swapped, and the new imaginary part is negated, in order to effect a 90° phase shift in the detection (t_2) dimension. Finally, these two FIDs are used as the complex pair for two-dimensional Fourier transformation. Quadrature images in F1 occur if the two coherence transfer pathways are not identical, due to pulse imperfections or relaxation effects (*6, 8*). The theoretical analysis of the TROSY experiment indicates that nuclear spin relaxation affects the cosine- and sine-modulated components equally, and the absence of F1 quadrature images due to pulse imperfections or other effects in spectra acquired and processed in this manner was verified experimentally using the sample of calbindin D_{9k} (data not shown).

As mentioned under Theory, the equilibrium ^{15}N polarization can contribute to the desired TROSY resonances and improve sensitivity; therefore care must be taken to ensure that the signals arising from the initial ^{15}N polarization are additive to those originating from the ^{1}H polarization (*1*). In addition, the phases of the proton pulses must be selected such that the water magnetization is placed along the $+z$ axis after the final proton 90° pulse in the water flip-back experiment. Unfortunately, due to different conventions among spectrometer manufacturers, the RF phases needed to achieve the desired results can differ among instruments. The RF phases listed in Fig. 1 and discussed in the text are appropriate for the Varian INOVA spectrometer. The first proton 180° pulse has been changed from x to y, and the receiver phase cycling has been altered, compared with the original TROSY sequence reported by Pervushin *et al.* (*1*). For data collection on a Bruker DRX spectrometer, the phase of the second proton 90° pulse should be changed from $+y$ to $-y$, and the two four-step receiver phase cycles should be changed to $\phi_4 = (+x, -x, -y, +y)$ and $(-x, +x, -y, +y)$.

RESULTS AND DISCUSSION

A contour plot of the ^{1}H–^{15}N TROSY spectrum of the [^{2}H, ^{15}N]-labeled protein TIM is presented in Fig. 2; the data were acquired with the sensitivity-enhanced, water flip-back pulse sequence shown in Fig. 1b, and acquisition parameters are given in the legend to Fig. 2. Figure 3 shows slices taken parallel to the F1 axis from a conventional TROSY spectrum of TIM (TROSY), the sensitivity-enhanced TROSY spectrum (SE-TROSY), and the sensitivity-enhanced, water flip-back TROSY spectrum (SE/FB-TROSY). All spectra were recorded using the same total acquisition time. The slices are plotted such that the baseline noise has the same amplitude for all three spectra in order to facilitate visual assessment of the relative sensitivities of the three experiments.

The average relative signal-to-noise ratios for 53 resonances chosen at random were 1.0, 1.4, and 2.2 for the three spectra, respectively. The PEP approach yields the theoretically expected $\sqrt{2}$ gain in sensitivity. By avoiding saturation transfer from water protons, the water flip-back pulse sequence provides an additional 53% sensitivity gain.

The sensitivity gain afforded by the water flip-back technique depends on the length of the recycle delay compared to the water proton T_1 and will be larger for shorter recycle

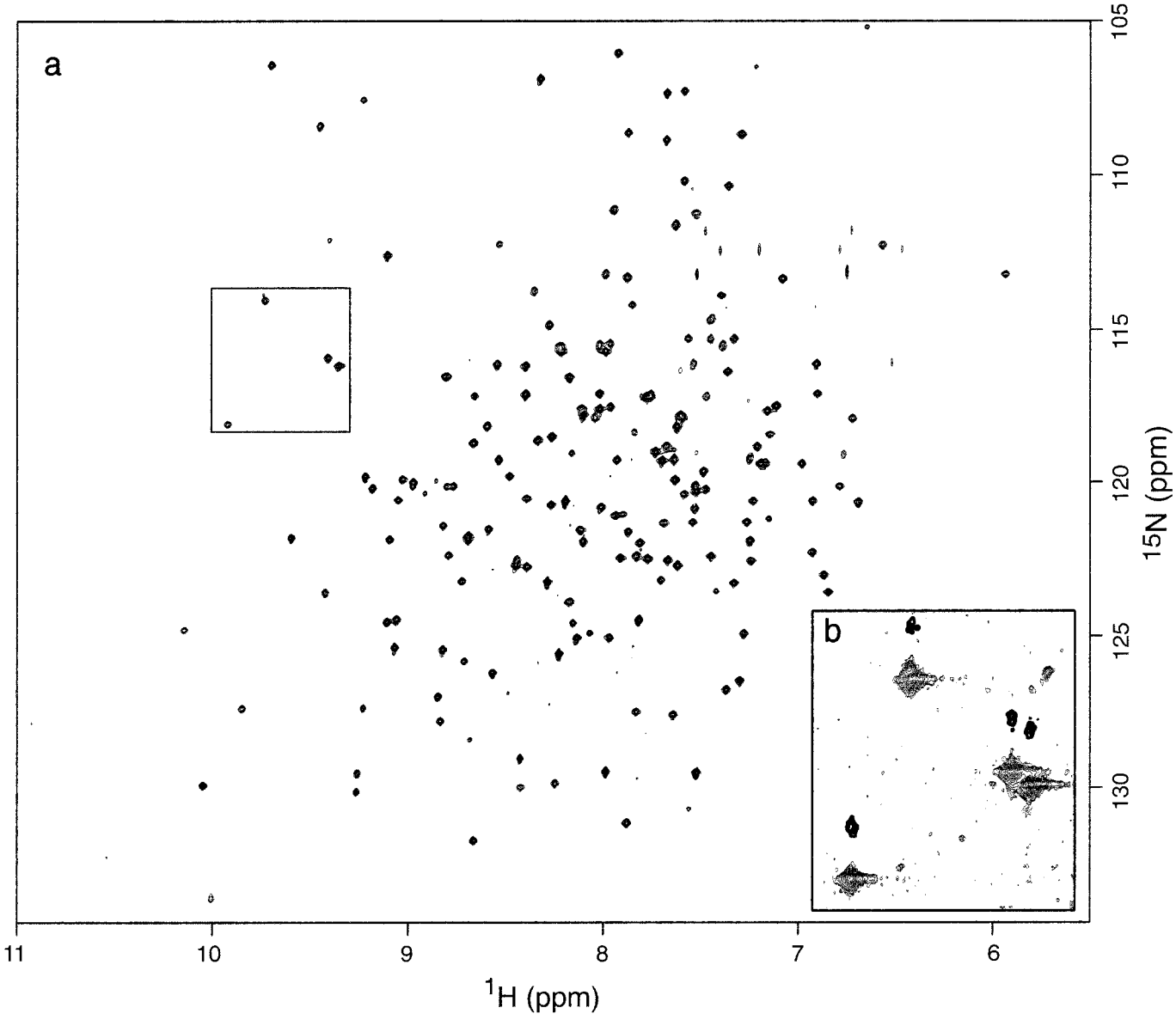

FIG. 2. ^{1}H–^{15}N TROSY spectrum at 303 K of (W90Y, W157F) double mutant triosephosphate isomerase (TIM) randomly 45% fractionally enriched with ^{2}H at nonexchangeable sites. (a) The water flip-back, sensitivity-enhanced ^{1}H–^{15}N TROSY spectrum acquired at 800 MHz using the pulse sequence of Fig. 1b is shown. (b) An expansion of the boxed region in (a) is drawn at a lower contour threshold to illustrate the negative multiplet components observed for some resonances. The boxed region extends from 112.7 to 119.3 ppm in F1 and from 9.2 to 10.1 ppm in F2. Only positive contours are shown in (a), while negative contours are drawn in heavy lines in (b). The spectrum was acquired using 4 scans for each recorded FID (16 scans per t_1 increment), 320 complex t_1 increments, and (F1, F2) spectral widths of (2500 Hz, 15609.76 Hz). To facilitate comparisons with the conventional sequence, quadrature detection in the F1 dimension was achieved by repeating data collection for each t_1 value with RF phase ϕ_1 incremented by 90° to provide a hypercomplex data set. The required manipulation of the FIDs prior to Fourier transformation is described in the text.

delays. The data shown in Fig. 3 were obtained using a 2.5-s recycle delay (compared with a water proton T_1 of ~4 s). Figure 4 illustrates the sensitivity difference between the SE-TROSY and SE/FB-TROSY as a function of the recycle delay. As expected, the SE/FB-TROSY is much more sensitive than the SE-TROSY for short recycle delays, but both experiments give essentially identical results for recycle delays much greater than the water proton T_1. The increase in sensitivity associated with the water flip-back procedure is fairly uniform for different resonances in the spectrum of TIM. This is somewhat surprising because amide protons involved in intramolecular hydrogen bonds would be expected to exchange slowly with solvent. However, the large molecular mass and long rotational correlation time of TIM results in very effective spin diffusion that transfers saturation among protons (*33*), even in the fractionally deuterated

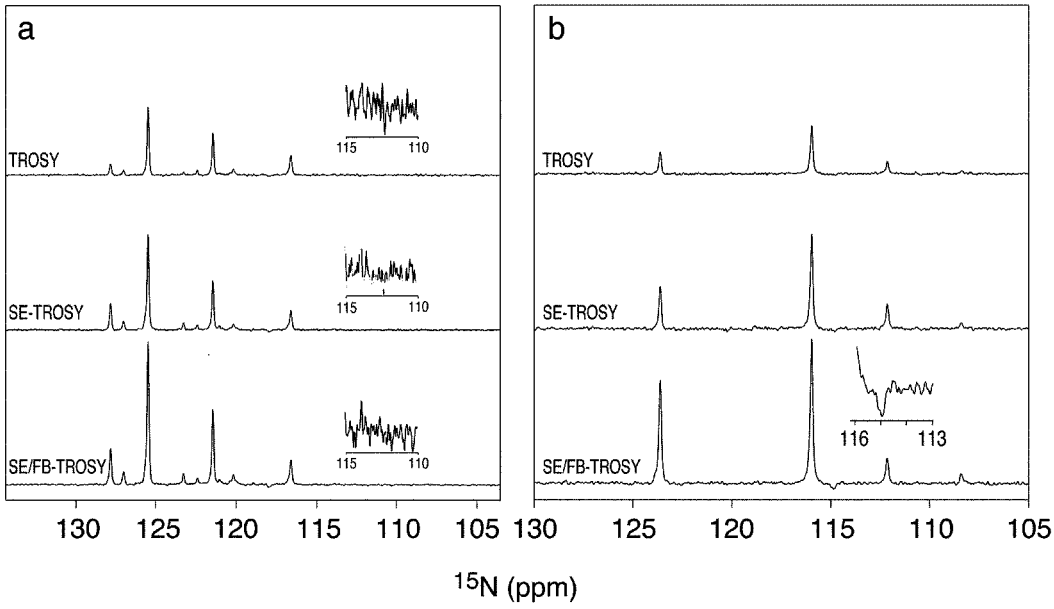

FIG. 3. Sensitivity of TROSY spectra. One-dimensional slices parallel to the F1 axis are shown for the TROSY, sensitivity-enhanced TROSY (SE-TROSY), and sensitivity-enhanced water flip-back TROSY (SE/FB-TROSY) spectra of TIM. Conventional and sensitivity-enhanced TROSY spectra were acquired using the same parameters as for the SE/FB-TROSY spectrum depicted in Fig. 2. The conventional TROSY spectrum was obtained from the SE-TROSY data by addition of the two FIDs recorded for each value of ϕ_1 and t_1. Slices are taken at (a) 8.82 ppm and (b) 9.42 ppm. The spectra are scaled so that the noise level is identical for each slice in (a) and for each slice in (b) to facilitate sensitivity comparisons. The baseline regions between 110 and 115 ppm are expanded vertically to show the noise levels in the spectra in (a). The region between 113 and 116 ppm is expanded vertically for the SE/FB-TROSY spectrum in (b) to illustrate the weak negative multiplet component at $(\Omega_H - \pi J_{NH}, \Omega_N - \pi J_{NH})$ corresponding to amplitude factor ϵ_2.

molecule. This effect will be reduced in proteins more highly enriched in deuterium.

The theoretical analysis of relaxation effects during the TROSY refocusing period indicates that the differences among the relaxation rate constants for ^{1}H single-quantum coherence, ^{15}N single-quantum coherence, and multiple-quantum coherence can result in the appearance of additional resonances at the frequencies of undesired spin multiplet components. The

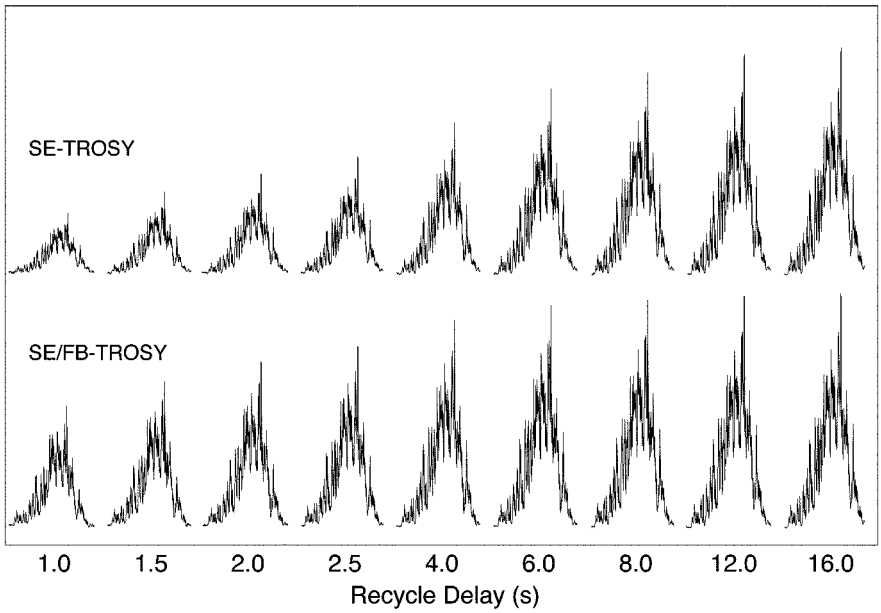

FIG. 4. Effect of recycle delay length on TROSY spectra. The signal intensities in the first FIDs of the (top) sensitivity-enhanced and (bottom) sensitivity-enhanced water flip-back TROSY spectra of TIM are shown as a function of the recycle delay ranging from 1 to 16 s.

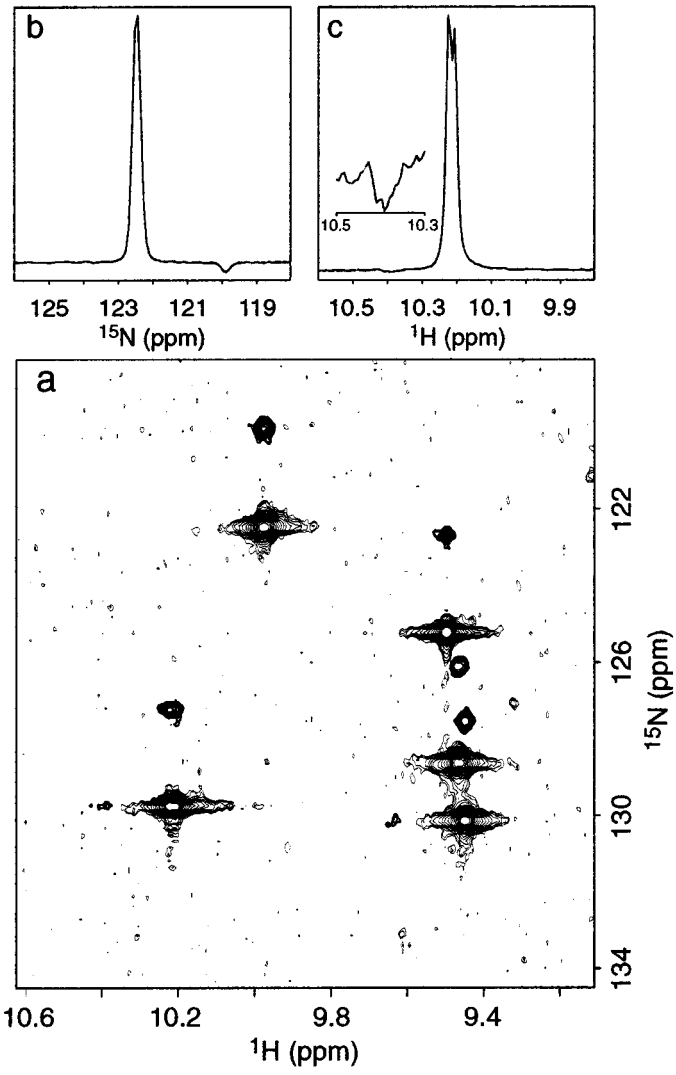

FIG. 5. TROSY spectrum of calbindin D_{9k} at 303 K. (a) A section of the water flip-back, sensitivity-enhanced ^{1}H–^{15}N TROSY spectrum acquired at 500 MHz using the pulse sequence of Fig. 1b is shown to illustrate residual multiplet components originating from relaxation-induced imbalance during the TROSY refocusing period. Positive contours are shown as thin lines and negative contours are shown as heavy lines. The spectrum was acquired using 4 scans for each recorded FID (16 scans per t_1 increment), 256 complex t_1 increments, and (F1, F2) spectral widths of (1600 Hz, 12527.4 Hz). The RF phase ϕ_1 was incremented by 90° to achieve F1 quadrature detection. (b) A slice parallel to the F1 axis at F2 = 9.97 ppm is shown to illustrate the negative multiplet at frequency coordinates ($\Omega_H - \pi J_{NH}$, $\Omega_N - \pi J_{NH}$) corresponding to amplitude factor ϵ_2. (c) A slice parallel to the F2 axis at F1 = 129.7 ppm is provided to show the weak multiplet at frequency coordinates ($\Omega_H + \pi J_{NH}$, $\Omega_N + \pi J_{NH}$) corresponding to amplitude factor ϵ_3. The region between 10.3 and 10.5 ppm is expanded vertically to show the negative multiplet component more clearly.

largest additional component is predicted to occur at ($\Omega_N - \pi J_{NH}$, $\Omega_H - \pi J_{NH}$) with amplitude ϵ_2, and is negative as long as $R_{MQ} > R_2$. This resonance is visible for a subset of the signals in the TROSY spectrum of TIM, as shown in Fig. 2b and in Fig. 3b. The smaller of the additional multiplet components is predicted to occur at ($\Omega_N + \pi J_{NH}$, $\Omega_H + \pi J_{NH}$) with amplitude ϵ_3. This resonance is too weak to be observed in Fig. 2. Equation [16] predicts that ϵ_2 is larger for fully protonated molecules, and Eq. [17] predicts that ϵ_3 is larger at lower magnetic fields. Figure 5 illustrates a subsection of the TROSY spectrum acquired at 500 MHz for ^{15}N-labeled calbindin D_{9k}. Both the large negative resonance at ($\Omega_N - \pi J_{NH}$, $\Omega_H - \pi J_{NH}$) and the weak negative resonance at ($\Omega_N + \pi J_{NH}$, $\Omega_H + \pi J_{NH}$) can be observed. The relaxation rate constants at 500 MHz for ^{15}N-labeled calbindin D_{9k} were estimated from Eqs. [5]–[9] using $\tau_m = 4.25$ ns and $r_{IS} = 1.02$ Å, r_{IK} obtained from the atomic coordinates of the molecule (PDB file 2bca), $\sigma_I = -16$ ppm, and $\sigma_S = -160$ ppm (*1*). The calculated values of $R_{2I} = 22.6\ s^{-1}$, $R_{2S} = 10.0\ s^{-1}$, and $R_{MQ} = 19.2\ s^{-1}$ yield $\epsilon_1 = 0.81$, $\epsilon_2 = -0.025$, and $\epsilon_3 = -0.009$. The relative intensities of the additional multiplet components compared with the TROSY resonance are $\epsilon_2/\epsilon_1 = -0.031$ and $\epsilon_3/\epsilon_1 = -0.011$. As can be seen, the calculated intensities predict the signs and qualitative magnitudes of the two additional multiplet components. In some instances, for example, three-dimensional NOESY spectra of protonated molecules in which TROSY techniques are used for spectral editing, the negative multiplet components may interfere with accurate quantification.

CONCLUSION

The recently developed TROSY technique (*1*) utilizes interference between the DD and CSA relaxation mechanisms to obtain substantially increased resolution and sensitivity in ^{1}H–^{15}N heteronuclear correlation spectra of large biological macromolecules at very high static magnetic fields. As demonstrated herein, by implementing the PEP and water flip-back schemes in the TROSY pulse sequence, the sensitivity of the experiment is increased by more than $\sqrt{2}$, which corresponds to a reduction in experimental acquisition time by more than a factor of 2. The increased sensitivity per unit time will be valuable particularly for large macromolecules and molecules of limited solubility or stability. The twofold shorter phase cycle that can be used with the PEP scheme also facilitates incorporation of the TROSY method in other more complex three- and four-dimensional experiments.

ACKNOWLEDGMENTS

We thank Dr. Walter Chazin (Scripps Research Institute) for providing the sample of calbindin D_{9k} and Dr. Ann McDermott (Columbia University) for providing the expression plasmid for triosephosphate isomerase. This work was supported in part by Grant GM40089 (M.R.) and National Research Service Award GM19247 (J.P.L.) from the National Institutes of Health, and the Searle Scholars Program (A.G.P.).

REFERENCES

1. K. Pervushin, R. Riek, G. Wider, and K. Wüthrich, Attenuated T_2 relaxation by mutual cancellation of dipole–dipole coupling and chemical shift anisotropy indicates an avenue to NMR structures of very large biological macromolecules in solution, *Proc. Natl. Acad. Sci. USA* **94,** 12366–12371 (1997).

2. M. Goldman, Interference effects in the relaxation of a pair of unlike spin-1/2 nuclei, *J. Magn. Reson.* **60,** 437–452 (1984).
3. H. Shimizu, Theory of the dependence of nuclear magnetic relaxation on the absolute sign of spin–spin coupling constant, *J. Chem. Phys.* **40,** 3357–3364 (1964).
4. M. Guéron, J. L. Leroy, and R. H. Griffey, Proton nuclear magnetic relaxation of ^{15}N-labeled nucleic acids via dipolar coupling and chemical shift anisotropy, *J. Am. Chem. Soc.* **105,** 7262–7266 (1983).
5. R. H. Griffey and A. G. Redfield, Proton-detected heteronuclear edited and correlated nuclear magnetic resonance and nuclear Overhauser effect in solution, *Q. Rev. Biophys.* **19,** 51–82 (1987).
6. J. Cavanagh and M. Rance, Sensitivity improvement in isotropic mixing (TOCSY) experiments, *J. Magn. Reson.* **88,** 72–85 (1990).
7. M. Rance, Sensitivity improvement in multi-dimensional NMR spectroscopy, *Bull. Magn. Reson.* **16,** 54–67 (1994).
8. A. G. Palmer, J. Cavanagh, P. E. Wright, and M. Rance, Sensitivity improvement in proton-detected two-dimensional heteronuclear correlation NMR spectroscopy, *J. Magn. Reson.* **93,** 151–170 (1991).
9. A. G. Palmer, J. Cavanagh, R. A. Byrd, and M. Rance, Sensitivity improvement in three-dimensional heteronuclear correlation NMR spectroscopy, *J. Magn. Reson.* **96,** 416–424 (1992).
10. N. J. Skelton, A. G. Palmer, M. Akke, J. Kördel, M. Rance, and W. J. Chazin, Practical aspects of two-dimensional proton-detected ^{15}N spin relaxation measurements, *J. Magn. Reson. B* **102,** 253–264 (1993).
11. L. E. Kay, P. Keifer, and T. Saarinen, Pure absorption gradient enhanced heteronuclear single quantum correlation spectroscopy with improved sensitivity, *J. Am. Chem. Soc.* **114,** 10663–10665 (1992).
12. M. Akke, P. A. Carr, and A. G. Palmer, Three-dimensional heteronuclear NMR spectroscopy with simultaneous isotope filtration, quadrature detection and sensitivity enhancement using *z*-rotation pulses, *J. Magn. Reson. B* **104,** 298–302 (1994).
13. J. Schleucher, M. Schwendinger, M. Sattler, P. Schmidt, O. Schedletzky, S. J. Glaser, O. W. Sørensen, and C. Griesinger, A general enhancement scheme in heteronuclear multidimensional NMR employing pulsed field gradients, *J. Biomol. NMR* **4,** 301–306 (1994).
14. O. W. Sørensen, G. W. Eich, M. H. Levitt, G. Bodenhausen, and R. R. Ernst, Product operator formalism for the description of NMR pulse experiments, *Prog. NMR Spectrosc.* **16,** 163–192 (1983).
15. F. J. M. van de Ven and C. W. Hilbers, A simple formalism for the description of multiple-pulse experiments. Application to a weakly coupled two-spin ($I = \frac{1}{2}$) system, *J. Magn. Reson.* **54,** 512–520 (1983).
16. K. J. Packer and K. M. Wright, The use of single-spin operator basis sets in the NMR spectroscopy of scalar-coupled spin systems, *Mol. Phys.* **50,** 797–813 (1983).
17. J. Cavanagh, W. J. Fairbrother, A. G. Palmer, and N. J. Skelton, "Protein NMR Spectroscopy: Principles and Practice," Academic Press, San Diego (1996).
18. A. Abragam, "Principles of Nuclear Magnetism," Clarendon Press, Oxford (1961).
19. A. G. Palmer, N. J. Skelton, W. J. Chazin, P. E. Wright, and M. Rance, Suppression of the effects of cross-correlation between dipolar and anisotropic chemical shift relaxation mechanisms in the measurement of spin–spin relaxation rates, *Mol. Phys.* **75,** 699–711 (1992).
20. L. Müller and R. R. Ernst, Coherence transfer in the rotating frame. Application to heteronuclear cross-correlation spectroscopy, *Mol. Phys.* **38,** 963–992 (1979).
21. S. Grzesiek and A. Bax, The importance of not saturating H_2O in protein NMR. Application to sensitivity enhancement and NOE measurements, *J. Am. Chem. Soc.* **115,** 12593–12594 (1993).
22. J. Stonehouse, G. L. Shaw, J. Keeler, and E. D. Laue, Minimizing sensitivity losses in gradient-selected ^{15}N–^{1}H HSQC spectra of proteins, *J. Magn. Reson. A* **107,** 178–184 (1994).
23. L. E. Kay, G. Y. Xu, and T. Yamazaki, Enhanced-sensitivity triple-resonance spectroscopy with minimal H_2O saturation, *J. Magn. Reson. A* **109,** 129–133 (1994).
24. S. Mori, C. Abeygunawardana, M. O'Neil Johnson, and P. C. M. van Zijl, Improved sensitivity of HSQC spectra of exchanging protons at short interscan delays using a new fast HSQC (FHSQC) detection scheme that avoids water saturation, *J. Magn. Reson. B* **108,** 94–98 (1995).
25. V. Sklenář, M. Piotto, R. Leppik, and V. Saudek, Gradient-tailored water suppression for ^{1}H–^{15}N HSQC experiments optimized to retain full sensitivity, *J. Magn. Reson. A* **102,** 241–245 (1993).
26. M. Liu, X.-a. Mao, C. Ye, H. Huang, J. K. Nicholson, and J. C. Lindon, Improved WATERGATE pulse sequences for solvent suppression in NMR spectroscopy, *J. Magn. Reson.* **132,** 125–129 (1998).
27. M. Piotto, V. Saudek, and V. Sklenář, Gradient-tailored excitation for single-quantum NMR spectroscopy of aqueous solutions, *J. Biomol. NMR* **2,** 661–665 (1992).
28. A. Bax, M. Ikura, L. E. Kay, and G. Zhu, Removal of F_1 baseline distortion and optimization of folding in multidimensional NMR spectra, *J. Magn. Reson.* **91,** 174–178 (1991).
29. J. Sambrook, E. F. Fritsch, and T. Maniatis, "Molecular Cloning," Cold Spring Harbor Laboratory Press, Cold Spring Harbor, NY (1989).
30. E. A. Komives, L. C. Chang, E. Lolis, R. F. Tilton, G. A. Petsko, and J. R. Knowles, Electrophilic catalysis in triosephosphate isomerase: The role of histidine-95, *Biochemistry* **30,** 3011–3019 (1991).
31. S. J. Putman, A. F. Coulson, I. R. Farley, B. Riddleston, and J. R. Knowles, Specificity and kinetics of triose phosphate isomerase from chicken muscle, *Biochem. J.* **129,** 301–310 (1972).
32. J. C. Williams and A. E. McDermott, Dynamics of the flexible loop of triosephosphate isomerase: The loop motion is not ligand gated, *Biochemistry* **34,** 8309–8319 (1995).
33. J. D. Stoesz, A. G. Redfield, and D. Malinowski, Cross relaxation and spin diffusion effects on the proton NMR of biopolymers in H_2O, *FEBS Lett.* **91,** 320–324 (1978).